Thermal footprint of a boundary layer with a step change in roughness

By S. Vijay AND B.J. McKeon

Surface roughness significantly affects both thermal and momentum transport in turbulent flows, yet their coupled behavior, particularly under nonequilibrium conditions, remains less well understood. This experimental study, conducted in a low-speed wind tunnel using infrared thermography and a modular heated-wall system, investigates the evolving thermal footprint of a turbulent boundary layer subjected to a step change in roughness. Two types of test surfaces are used: a smooth surface made of a 0.8-mm-thick copper plate and a rough surface 3D-printed using direct metal laser sintering (DMLS) manufactured from an aluminum–silicon–magnesium alloy (AlSiMg). The rough wall shows consistently higher Stanton numbers compared with both the smooth wall and theoretical predictions. Temperature fields show that surface roughness enhances convective transport and produces a persistent downstream thermal imprint, highlighting the influence of geometric heterogeneity on scalar–momentum coupling in nonequilibrium turbulent flows.

1. Introduction

Rough surfaces are ubiquitous in nature, and considerable research effort has been devoted to understanding the effects of wall surfaces on momentum and scalar transport in turbulent flows. Many engineering applications, such as flow over canopies, iced airfoils, or damaged turbine blades (Kadivar *et al.* 2021), involve irregular roughness across a wide range of scales, which introduces strong spatial heterogeneity. Of particular interest are abrupt surface changes, such as transitions in roughness or heating, that drive boundary layers into nonequilibrium states. The transport of momentum and passive scalar (e.g., heat, pollutant concentration, salinity) in a fluid is traditionally considered analogous and is based on the idea that the same turbulent eddies transport both scalar quantities and momentum for a given viscosity and scalar diffusivity of the fluid. The Reynolds analogy factor (RA), representing the ratio of twice the Stanton number (St) to the skin-friction coefficient (C_f), helps quantify the relationship between passive scalar transport and momentum transport. RA is expressed as a function of the skin-friction coefficient (C_f) and the difference between the velocity and temperature roughness functions ($\Delta U^+ - \Delta\Theta^+$). Therefore, the Reynolds analogy holds when $\Delta U^+ - \Delta\Theta^+ = 0$, whereas it breaks down on the negative side when $\Delta U^+ - \Delta\Theta^+ > 0$.

The Reynolds analogy has been extensively verified for smooth walls; however, for rough walls, while C_f achieves a constant value in the fully rough regime, St remains sensitive to scalar diffusivity and decreases with increasing Reynolds number (Hantsis & Piomelli 2020). An analysis of instantaneous temperature fields suggested that the dissimilarity between heat and momentum transfer arises because the pressure drag acting on the rough wall enhances momentum transfer but not heat transfer (Chung *et al.* 2021; Kuwata 2022), implying a breakdown of the Reynolds analogy when the surface is sufficiently rough. Understanding the mechanisms related to this breakdown is crucial,

as the introduction of RA helps quantify the discrepancy between momentum and heat transfer.

Direct numerical simulation (DNS) offers unparalleled access to flow and scalar variables, providing insight into turbulence statistics and the physics of turbulent heat transfer (Hantsis & Piomelli 2022, 2020; MacDonald *et al.* 2019). However, performing DNS for rough wall turbulence at higher Reynolds numbers remains computationally intensive because of the need to resolve boundary layer and roughness elements. Suggestions that empirical coefficients for correlation may depend on rough surface characteristics underscore the necessity of additional investigations to derive a universal correlation for generic rough surfaces (Forooghi *et al.* 2018), emphasizing the need for a comprehensive understanding of the underlying physics of wall roughness effects on heat transfer. In particular, for irregular rough surfaces, k_s can vary on the basis of roughness topography, considering factors such as frontal solidity (λ_p), effective slope (ES), skewness (Sk), and root-mean-square height (k_{rms}) (Chung *et al.* 2021). For example, recent efforts by Yang *et al.* (2025) introduced a surface anisotropy ratio (SAR), defined as the ratio of streamwise to spanwise frontal solidity, to characterize directional roughness effects, showing that increasing the SAR enhances streamwise-aligned shear while suppressing scalar mixing, thereby intensifying the breakdown of the Reynolds analogy in anisotropic rough wall turbulence.

However, challenges in predicting skin friction in nonequilibrium flows, such as those that transition from rough to smooth surfaces or occur under strong adverse pressure gradients, suggest that similar complexities may arise in predicting heat transfer (García-Mayoral *et al.* 2024). In turbulent boundary layers, heat transfer becomes particularly complex under nonequilibrium conditions. The surface changes result in the formation of internal boundary layers (IBLs), while the outer flow retains its upstream history. In these spatially developing flows, the classical diffusion analogy (Miyake 1965) fails because scalar transport relies primarily on diffusive processes and form-induced fluxes, whereas momentum transport benefits from pressure-driven enhancement through form drag. Consequently, scalar IBLs exhibit systematically larger growth exponents than their momentum counterparts (Rouhi *et al.* 2019; MacDonald 2024), making scalar recovery less well understood in such nonequilibrium conditions. Furthermore, Jensen & Forooghi (2025) showed that patchy roughness generates secondary motions and IBLs whose recovery depends on the size and spacing of rough and smooth patches, highlighting the role of surface heterogeneity and patterning in nonequilibrium turbulence. It remains unclear how the history effects observed in velocity fields under varying pressure gradients may also manifest in temperature fields.

Various experimental studies have examined the response of thermal boundary layers to surface transitions, including smooth-to-rough changes (Antonia & Luxton 1971), step changes in wall temperature (Ligrani & Moffat 1985), and step changes in surface heat flux (Antonia *et al.* 1977), as well as combined roughness–temperature variations (Léon *et al.* 2020). These studies collectively show that abrupt surface changes generate IBLs and prolonged downstream adjustments of the thermal field, indicating that scalar recovery is intrinsically slower and more sensitive to wall heterogeneity than its momentum counterpart. More recent efforts have enabled direct, wall-resolved observations of such processes. Foroozan *et al.* (2025) demonstrated that high-speed infrared thermography can nonintrusively capture the spatiotemporal evolution of wall heat transfer, revealing streaklike thermal footprints associated with near-wall turbulent structures.

Building on this progress, this study experimentally investigates scalar–momentum

coupling in turbulent boundary layers subjected to rough-to-smooth and heated-to-unheated transitions. A modular heated-wall system generates controlled surface changes, while infrared thermography provides detailed surface temperature maps that reveal the evolving thermal footprint of the boundary layer. This approach enables spatially resolved, nonintrusive measurements of heat transfer, offering a new means of probing how the internal scalar boundary layer develops relative to the momentum boundary layer under nonequilibrium conditions. By connecting wall-based thermal measurements to the underlying flow dynamics, this study aims to clarify the mechanisms governing the breakdown of the Reynolds analogy over heterogeneous surfaces.

2. Methods

The experimental facility builds upon the design by Vijay & McKeon (2024). We utilize a low-speed subsonic wind tunnel at Stanford University (Figure 1(a)). The cross-sectional dimensions of the working test section are 0.75×0.75 m with a length of 1.45 m. This wind tunnel is configured as an open-loop facility and can achieve an average freestream velocity (U_∞) in the test section ranging from 2 m/s to 10 m/s. The experimental setup uses the full length of the test section ($L = 1.45$ m) to ensure fully developed flow conditions. The heated section consists of a 30-cm-wide plate, with wooden insulation blocks placed along the edges to minimize lateral heat loss. The core heating element is an adhesive-mount heater (McMaster-Carr), which is applied to an insulated base to provide a constant heat flux. A replaceable test surface is mounted on top of this assembly. The walls of the test section are made of thermally insulated material, and a trip wire is installed to promote boundary layer transition. Two types of test surfaces are used in this study: a smooth surface made of 0.8-mm-thick copper plate and a rough surface 3D-printed using Direct-metal laser sintering manufactured from AlSiMg. The roughness geometry was chosen to align with the DNS study conducted by Hantsis & Piomelli (2020). It consists of a k-type roughness comprising randomly oriented ellipsoids with semiaxes of k, $1.4k$, and $2k$, with $k = 0.8$ mm.

For the heated portion, a silicone heater was used to provide a constant heat flux with nominal values varying from 250 W/m^2 to 1000 W/m^2 for various values of freestream velocities for both the smooth case and the rough case. A steady-state procedure was used to capture data for calculating the convective heat transfer coefficients. We employed a FLIR A325sc thermovision infrared camera with a 10-mm lens. The camera is capable of generating a highly resolved 320×240 pixel map across the surface for a total viewing area of 0.45×0.62 m. The system was then monitored until steady state was achieved, which typically required 2 h of continuous operation, at which point a final data set was collected. At this point, temperature data were recorded for 30 s using the infrared camera at 10 Hz. This procedure was repeated for both the smooth and rough configurations.

3. Results

Temperature distributions are characterized for two configurations: smooth wall flow and rough wall flow. We first present results for two freestream velocities, $U_\infty = 6.5$ m/s ($Re_x \approx 3\times10^5$ at the leading edge of the heated region) and $U_\infty = 8.5$ m/s ($Re_x \approx 4\times10^5$ at the leading edge of the heated region), for two different heat fluxes, $q'' = 340$ W/m^2 and $q'' = 1000$ W/m^2. Figure 2 shows the spatial temperature distribution over the heated plate at steady-state conditions.

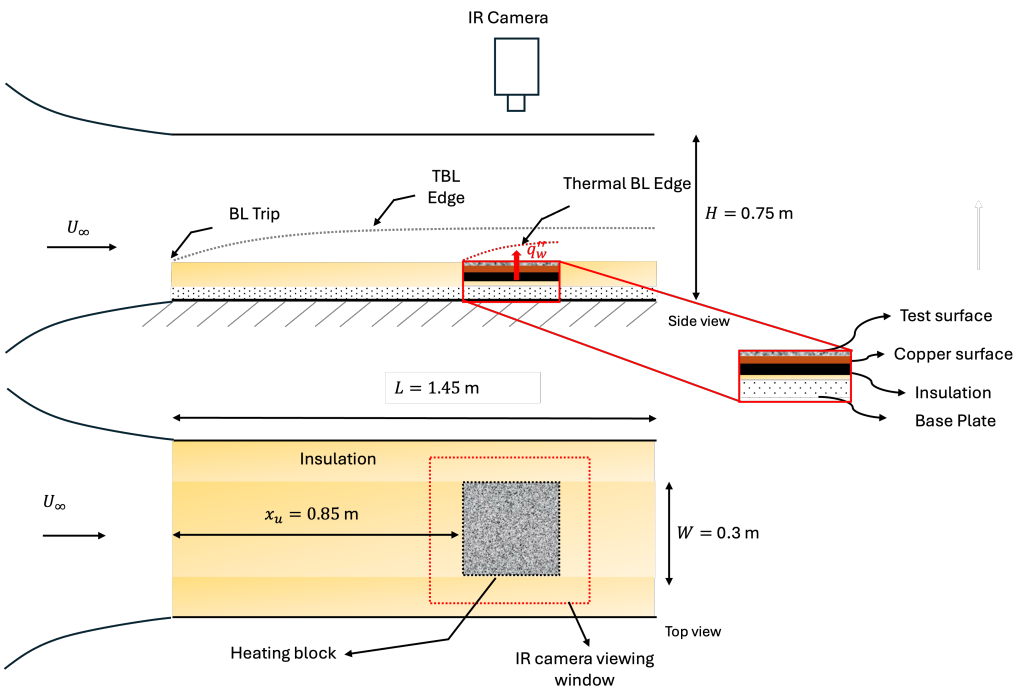

(a) Schematic of the experimental setup in the wind tunnel.

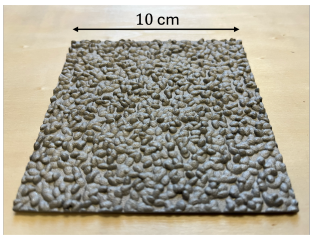

(b) Photograph of a single 3D-printed roughness tile used in the experiments, showing the as-fabricated surface texture and geometric features. The tile was manufactured using DMLS with AlSiMg.

Figure 1: Details of the experimental setup.

At each (i, j) pixel in the infrared image, the local convection coefficient was determined as follows

$$h_{i,j} = \frac{q''}{(T_{IR_{i,j}} - T_\infty)}, \tag{3.1}$$

where $T_{IR_{i,j}}$ is the temperature of the surface measured by the infrared camera, T_∞ is the freestream temperature, and q'' is the heat flux supplied by the heater. The local Stanton number is calculated as

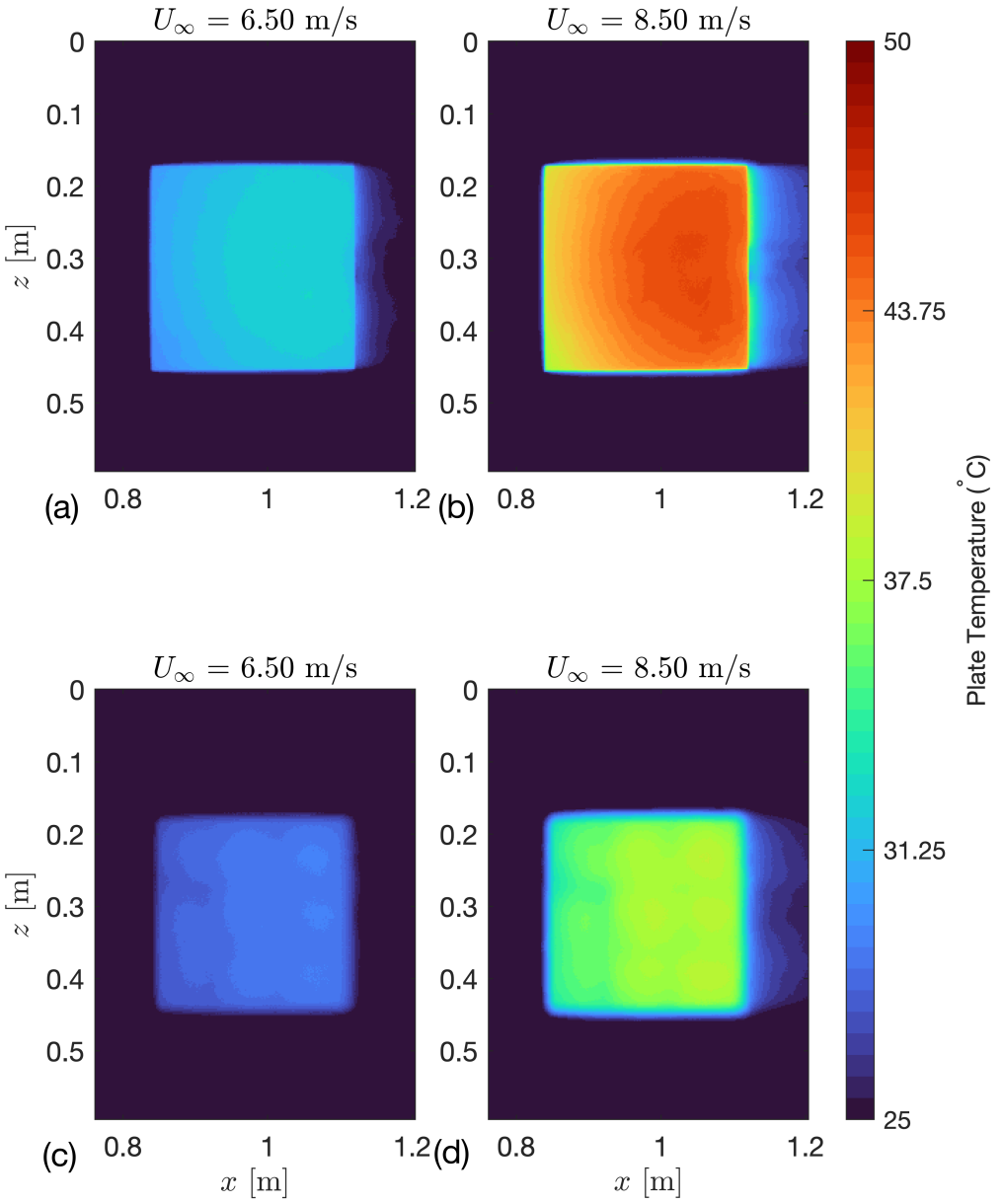

Figure 2: Steady-state surface temperature contours measured via infrared thermography. Panels (a) and (c) correspond to the smooth and rough wall configurations, respectively, at $U_\infty = 6.5\,\mathrm{m/s}$ and $q'' = 340$. Panels (b) and (d) correspond to the smooth and rough wall configurations, respectively, at $U_\infty = 8.5\,\mathrm{m/s}$ $q'' = 1000$. Figure reproduced from Vijay & McKeon (2025).

k_{max} (mm)	k_{rms} (mm)	Sk	ES
2.19	0.89	0.28	0.44

Table 1: Surface roughness statistics; k_{max} is the maximum peak-to-valley height of the roughness profile; k_{rms} is the root-mean-square roughness height; Sk is the skewness of the surface-height distribution; and ES is the effective slope, defined as the mean absolute gradient of the surface height.

$$St_{i,j} = \frac{h_{i,j}}{\rho_\infty U_\infty C_p}, \tag{3.2}$$

where ρ_∞ is the freestream density, U_∞ is the freestream velocity, and C_p is the specific heat at constant pressure. The measured Stanton numbers were also compared with theoretical predictions for turbulent boundary layer flow with a constant wall heat flux and corrections for an unheated starting length using the following expression from Ambrok *et al.* (1957).

$$St_{\text{turbulent}} = \left(1 - (\xi/x)^{9/10}\right)^{1/9} 0.0308\, Re_x^{-1/5}\, Pr^{-2/3}, \tag{3.3}$$

where ξ is the unheated starting length, x is the downstream distance from the leading edge, Re_x is the local Reynolds number based on x, and Pr is the Prandtl number. A similar analysis is performed for the rough surface. The Stanton number variation with Reynolds number is plotted in Figure **??** for $U_\infty = 6.5$ m/s and $U_\infty = 8.5$ m/s, respectively.

The temperature contours for the rough wall display more uniformity in the streamwise direction, indicating enhanced convective cooling. This results in a more uniform temperature distribution and a reduced streamwise temperature gradient compared with the smooth wall. The rough wall shows consistently higher Stanton numbers compared with both the smooth wall case and theoretical predictions. The elevated heat transfer is attributed to earlier boundary layer thinning and greater mixing induced by surface roughness. Notably, the experimental Stanton numbers exceed theoretical predictions for both the smooth and rough cases. This deviation is likely due to lateral heat conduction within the heated plate in comparison to the idealized one-dimensional convective model.

The smooth wall temperature maps exhibit a pronounced streamwise gradient and clear thermal development downstream of the heater. In contrast, the rough wall cases display more uniform streamwise temperature distributions, indicating enhanced convective mixing and reduced wall temperature rise. The thermal imprint of the rough surface persists several roughness heights downstream of the transition, implying that roughness effects extend beyond the heated section through continued scalar–momentum coupling.

Figure 4 shows temperature contours for $U_\infty \in [3.5, 4.5, 5.5, 6.5]$ at $q'' = 1000$ W/m^2. As the freestream velocity increases, the surface temperature gradients appear to flatten, suggesting stronger convective mixing and a reduction in streamwise temperature rise. The influence of the surface transition is more apparent in Figure 5, where a gradual

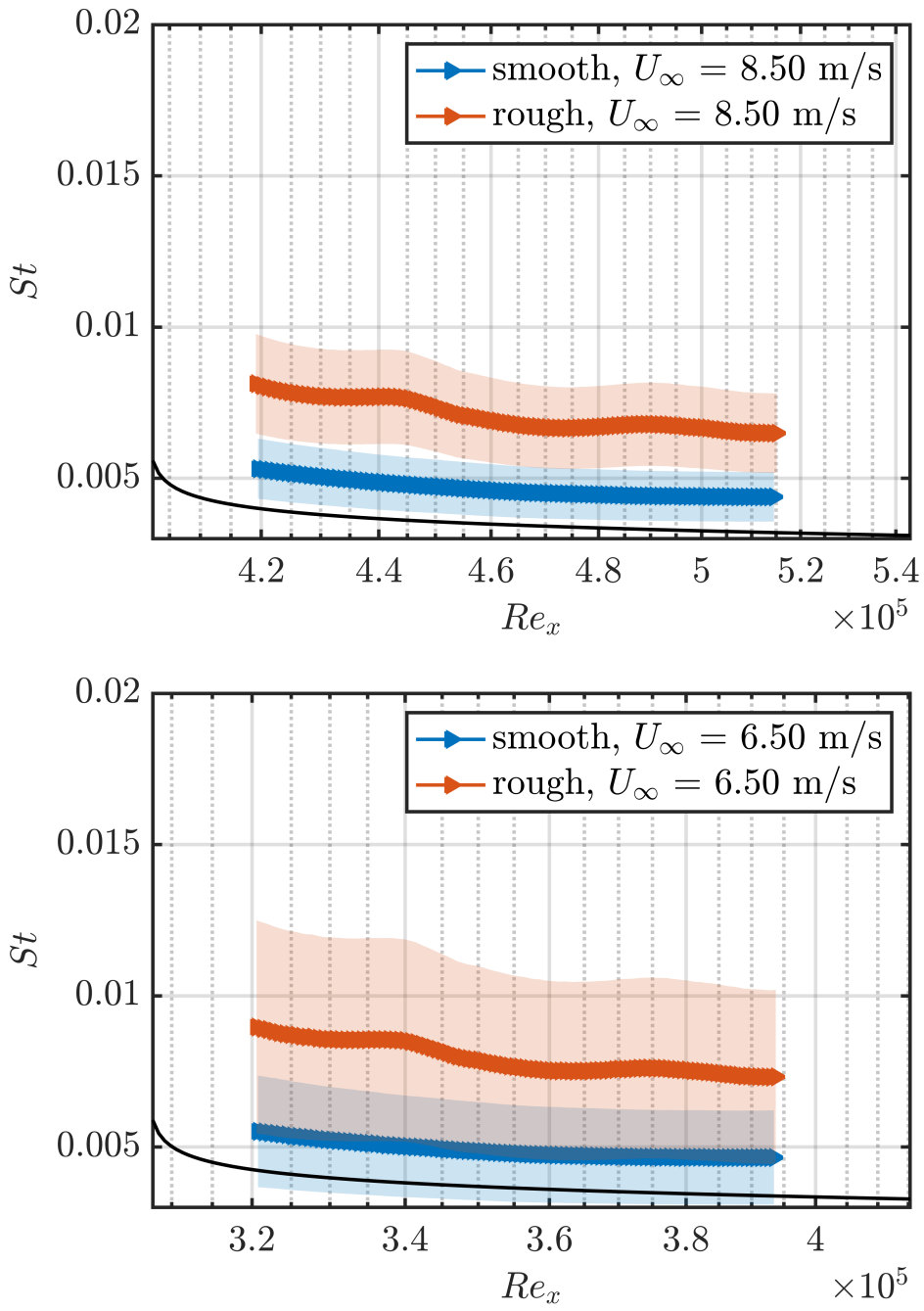

Figure 3: Centerline Stanton number (St) variations with local Reynolds number (Re_x) for $U_\infty = 6.5\,\mathrm{m/s}$ and $U_\infty = 8.5\,\mathrm{m/s}$. Each solid black line represents the theoretical prediction from Eq. (3.3). The shaded region is the experimental uncertainty.

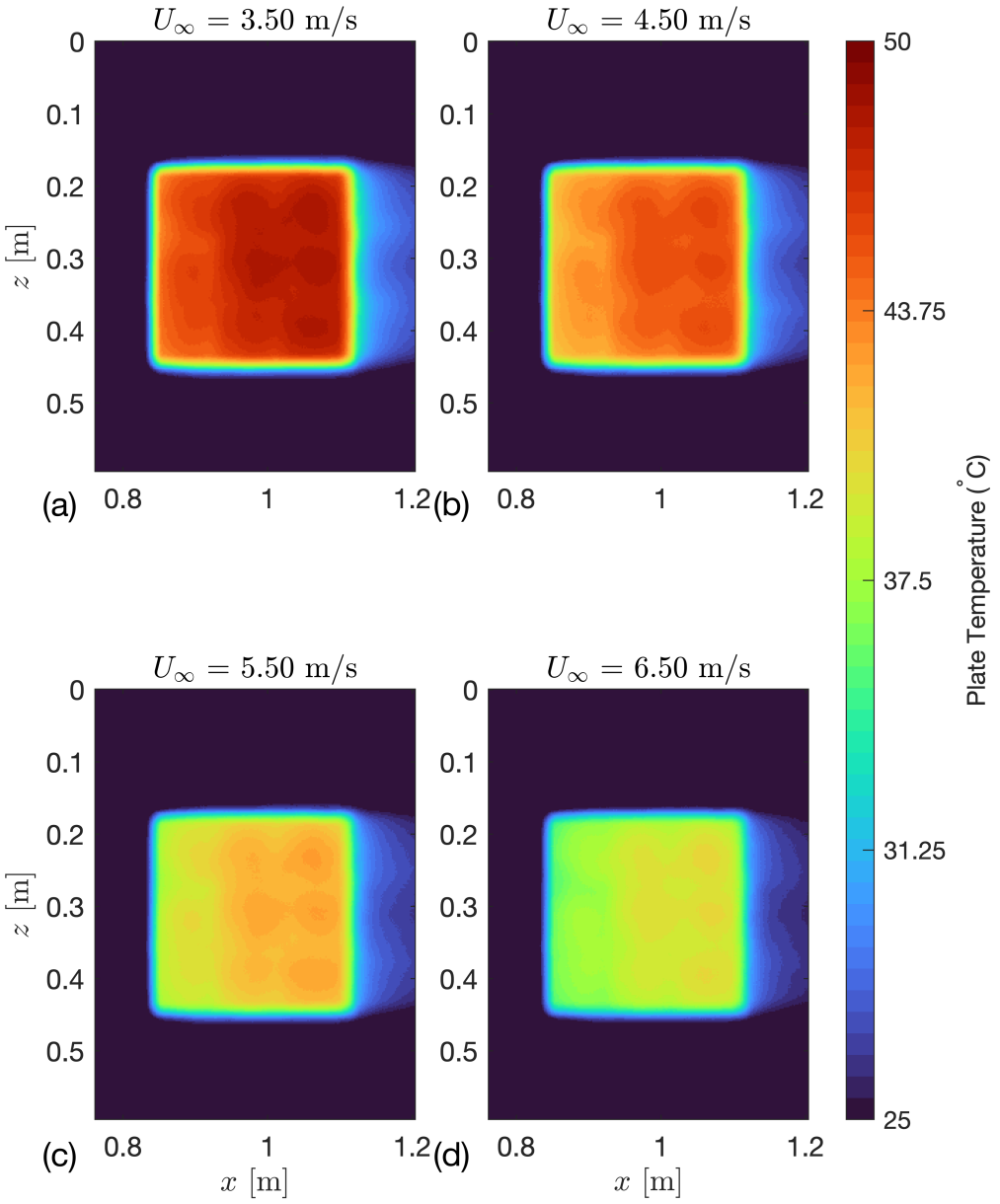

Figure 4: Steady-state surface temperature contours measured via infrared thermography for the same heat flux conditions ($q'' = 1000$ W/m^2) and increasing freestream velocity.

decay in wall temperature persists over a streamwise distance of approximately 50 mm. This persistence may indicate that the thermal imprint of the rough surface extends

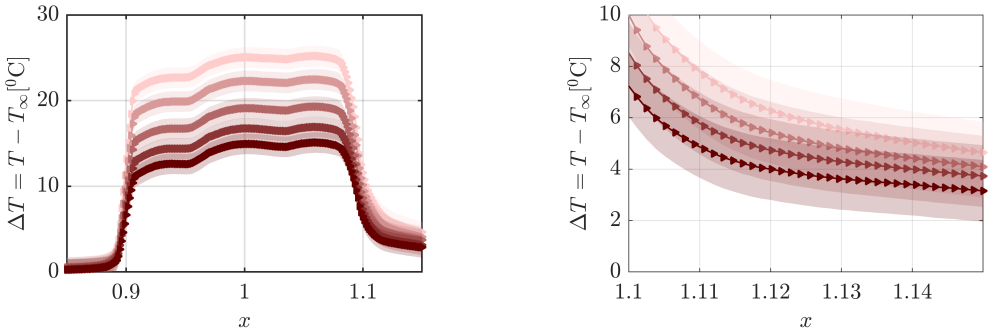

Figure 5: (a) Centerline mean temperature difference (ΔT) in the streamwise direction for various freestream velocities. Lighter shades correspond to lower velocities (U_∞ = 3.5 m/s), progressing to darker shades at higher velocities (U_∞ = 8.5 m/s). Increasing U_∞ reduces the streamwise temperature gradient and enhances convective mixing. (b) Magnified view of ΔT immediately downstream of the heated patch, highlighting the persistence of the thermal footprint and its gradual decay with distance.

beyond the heated section and that the boundary layer requires a finite downstream distance to reestablish equilibrium.

Qualitative comparisons with DNS can provide useful context. MacDonald (2024) reported that, following a roughness transition, the near-wall momentum field typically recovers within approximately 1–2 h downstream, whereas the scalar field retains upstream influence over more than 4 h. This slower adjustment of the scalar field was attributed to the longer timescale associated with diffusive and form-induced processes. The residual temperature variations observed here downstream of the rough region are qualitatively consistent with such behavior and may reflect a scalar IBL that has not yet fully adjusted to the local surface conditions.

A related interpretation emerges from simulations conducted by Jensen & Forooghi (2025), who examined turbulent flow over patchy roughness. They found that the influence of surface heterogeneity can persist for several boundary layer thicknesses (δ), with full equilibrium attained only after a streamwise distance of order $8\,\delta$. At smaller heterogeneity scales, secondary motions and dispersive stresses maintained nonequilibrium conditions. The continued thermal footprint observed in the present infrared data may similarly suggest that surface heterogeneity and localized secondary flows contribute to a delayed recovery of the thermal field. However, the infrared measurements capture only the wall-projected temperature field, providing limited information on how the scalar fluxes evolve with height. Wall-normal cold-wire measurements will therefore be essential to resolve the vertical distribution of temperature fluctuations and turbulent heat fluxes, enabling assessment of how deeply the effects of surface transitions and secondary motions penetrate into the flow and how the scalar field reequilibrates across the boundary layer.

4. Summary and outlook

The experiments described above show that surface roughness modifies wall–scalar coupling by enhancing local heat transfer and reducing streamwise temperature gradients, resulting in elevated Stanton numbers that exceed smooth wall predictions. The persistence of wall temperature variations downstream of roughness suggests the formation of an internal scalar boundary layer that adjusts more slowly than its momentum counterpart. This behavior appears to be qualitatively consistent with the DNS results obtained by MacDonald (2024) and Jensen & Forooghi (2025), who reported extended downstream influence of roughness transitions and surface heterogeneity over several roughness heights or boundary layer thicknesses.

Future experimental efforts will build on these findings to achieve higher spatiotemporal resolution of wall–scalar interactions. Recent experimental advances have made it possible to study these interactions directly at the wall. Foroozan *et al.* (2025) demonstrated that high-speed infrared thermography can nonintrusively resolve the spatiotemporal evolution of wall heat transfer and quantify instantaneous Nusselt number fluctuations, Nu'. Similar high-temporal-resolution infrared measurements in the present configuration could help capture the dynamics of thermal structures and their evolution downstream of surface transitions. In parallel, wall-normal cold-wire thermometry will be pursued to measure temperature fluctuations and turbulent heat fluxes across the boundary layer, providing complementary information on the vertical redistribution of scalar energy. Together, these approaches will enable a more complete characterization of how surface geometry, secondary motions, and nonequilibrium effects govern the coupled evolution of momentum and scalar transport over heterogeneous surfaces.

Acknowledgments

Support from the Office of Naval Research to the Center for Turbulence Research (grant N000142312833) is gratefully acknowledged. The authors thank Adrian Loekman for his assistance in collecting the experimental data.

REFERENCES

Ambrok, G. *et al.* 1957 Approximate solution of equations for the thermal boundary layer with variations in boundary layer structure. *Soviet Phys.-Tech. Phys* **2** (9), 1979–1986.

Antonia, R. A., Danh, H. Q. & Prabhu, A. 1977 Response of a turbulent boundary layer to a step change in surface heat flux. *J. Fluid. Mech.* **80**, 153–177.

Antonia, R. A. & Luxton, R. E. 1971 The response of a turbulent boundary layer to a step change in surface roughness. I. Smooth to rough. *J. Fluid. Mech.* **48**, 721–761.

Chung, D., Hutchins, N., Schultz, M. P. & Flack, K. A. 2021 Predicting the drag of rough surfaces. *Annu. Rev. Fluid Mech.* **53**, 439–471.

Forooghi, P., Stroh, A., Schlatter, P. & Frohnapfel, B. 2018 Direct numerical simulation of flow over dissimilar, randomly distributed roughness elements: a systematic study on the effect of surface morphology on turbulence. *J. Fluid Mech.* **837**, 284–307.

Foroozan, F., Ianiro, A., Discetti, S. & Baars, W. J. 2025 Resolving convective velocities of turbulent boundary layer–induced convective heat transfer fluctuations at the wall. *Phys. Rev. Fluids* **10**, 094904.

García-Mayoral, R., Chung, D., Durbin, P., Hutchins, N., Knopp, T., McK-

eon, B. J., Piomelli, U. & Sandberg, R. D. 2024 Challenges and perspective on the modelling of high-Re, incompressible, non-equilibrium, rough-wall boundary layers. *J. Turbul.* **25**, 423–449.

Hantsis, Z. & Piomelli, U. 2020 Roughness effects on scalar transport. *Phys. Rev. Fluids* **5**, 114607.

Hantsis, Z. & Piomelli, U. 2022 Effects of roughness on the turbulent Prandtl number, timescale ratio, and dissipation of a passive scalar. *Phys. Rev. Fluids* **7**, 124601.

Jensen, R. M. & Forooghi, P. 2025 A study of turbulent flow over patchy roughness. *J. Fluid Mech.* **1006**, A28.

Kadivar, M., Tormey, D. & McGranaghan, G. 2021 A review on turbulent flow over rough surfaces: fundamentals and theories. *Int. J. Thermofluids* **10**, 100077.

Kuwata, Y. 2022 Dissimilar turbulent heat transfer enhancement by Kelvin–Helmholtz rollers over high-aspect-ratio longitudinal ribs. *J. Fluid Mech.* **952**, A21.

Léon, O., Mollicone, J.-P., Battaglia, F., Dejoan, A., Laval, J.-P. & Stanislas, M. 2020 Aerodynamic and heat transfer effects of distributed surface roughness in turbulent boundary layers. *Int. J. Heat Fluid Flow* **85**, 108666.

Ligrani, P. M. & Moffat, R. J. 1985 Thermal boundary layer response to a step change in wall temperature. *Int. J. Heat Mass Transf.* **28**, 1519–1529.

MacDonald, M. 2024 Direct numerical simulation of momentum and scalar internal boundary layers. *Int. J. Heat Fluid Flow* **106**, 109285.

MacDonald, M., Hutchins, N., Lohse, D. & Chung, D. 2019 Heat transfer in rough-wall turbulent thermal convection in the ultimate regime. *Phys. Rev. Fluids* **4**, 071501(R).

Miyake, M. 1965 Transformation of the atmospheric boundary layer over inhomogeneous surfaces. Tech. Rep., Defense Technical Information Center.

Rouhi, A., Chung, D. & Hutchins, N. 2019 Direct numerical simulation of open-channel flow over smooth-to-rough and rough-to-smooth step changes. *J. Fluid Mech.* **866**, 450–486.

Vijay, S. & McKeon, B. J. 2024 Experimental investigation of heat transfer over roughness elements: design and preliminary results. In *Annual Research Briefs,* Center for Turbulence Research, Stanford University, pp. 195–202.

Vijay, S. & McKeon, B. J. 2025 Experimental investigation of turbulent heat transfer over roughness elements. In *Proceedings of the 11th International Symposium on Heat and Mass Transfer*. Heat Transfer Society of Japan.

Yang, J., Stroh, A., Bagheri, S., Frohnapfel, B. & Forooghi, P. 2025 Characterization of hydrodynamic and thermal properties of anisotropic irregular roughness. *Int. J. Heat Fluid Flow* **116**, 109888.